Catalytic Behavior of Graphite Nanofiber Supported Nickel Particles. 1. Comparison with Other Support Media

Alan Chambers, Tibor Nemes, Nelly M. Rodriguez, and R. Terry K. Baker*

Department of Chemistry, Northeastern University, Boston, Massachusetts 02115

Received: October 27, 1997; In Final Form: January 23, 1998

The hydrogenation of 1-butene and 1,3-butadiene has been carried out over a series of supported nickel catalysts at 80 °C and atmospheric pressure. It was found that not only the activity but also the selectivity of nickel crystallites could be dramatically altered when the metal was dispersed on graphite nanofibers compared to the performance obtained with more conventional support materials, such as active carbon and γ-alumina. Transmission electron microscopy examinations showed that the metal was evenly distributed over the graphite nanofiber surfaces, and in general the particles adopted a well-defined thin flat hexagonal shape. In contrast, the crystallites formed on active carbon and γ-alumina did not acquire the same well-defined morphological features; however, on average, they were considerably smaller than those generated on the nanofiber surfaces. The most dramatic feature was the fact that in the oxide supported nickel system the average particle size was about 5 times smaller than that for the same metal loading on the graphite nanofibers. Consideration of the particle size distributions in conjunction with the catalyst reactivity data indicates that hydrogenation of either 1-butene or 1,3-butadiene is not directly related to metal dispersion. It is suggested, instead, that differences in the behavioral patterns of the catalyst systems are related to the observed modifications in metal particle morphological characteristics induced by the chemical and structural properties of the support materials. In this context, consideration must also be given to the possibility that the support can induce electronic perturbations in the metallic component, and this feature could be most prominent with a conductive material such as graphite nanofibers.

Introduction

The concept of a metal−support interaction is one of the oldest in heterogeneous catalysis. In 1935, Adadurov[1] suggested that metals would be polarized by the surfaces of oxides containing highly charged cations. Although this idea did not appear to receive any immediate attention, it was probably the first suggestion of how the catalytic properties of a metal might be modified by the nature of the support phase. Oxide supports have been shown to alter the surface chemistry of metal catalyst particles through epitaxial, spillover, and migration effects.[2−6] The utilization of different carbonaceous supports with varying degrees of crystallinity, or graphitic nature, has also proven to be a fruitful method of transforming the performance of a given metal for selected probe reactions. Palladium decorated graphite specimens have been shown by Brownlie and co-workers to exhibit different selectivity patterns for simple hydrogenation reactions than that which was found from palladium deposited on a more disordered amorphous carbon support.[7] Gallezot and co-workers reported that platinum and ruthenium particles supported on graphite gave higher selectivities toward unsaturated alcohol in the hydrogenation of cinnamaldehyde than catalyst systems where these metals were supported on charcoal.[8,9] In these studies it was proposed that the metal clusters were selectively located on the basal plane of the graphite, which led to a strong interaction between the metal particles and the π-electrons of the support medium, and it was this feature that was responsible for the observed differences in catalyst performance.

While conventional forms of graphite offer some remarkable features as a catalyst support, the material suffers from a major shortcoming in that it has a relatively low surface area. In this context it is somewhat surprising to find that little attention has been devoted to the use of high surface area graphitized carbon fibers as a catalyst support. The inherent physical, mechanical, and chemical properties of carbon fibers would appear to make the material an attractive candidate for such an application. A Japanese patent published in 1973[10] describes one of the earliest attempts to utilize carbon fibers as a catalyst support for palladium. This catalyst system was used for the hydrogenation of cyclohexene and was claimed to maintain its activity for considerably longer periods of time than that found with catalysts prepared from palladium impregnated on conventional supports. The high electrical conductivity associated with graphitized carbon fibers opens up the possibility of introducing the metallic components by electrochemical techniques, an aspect that was exploited by Theodoridou and co-workers,[11] who deposited various noble metals onto such fibers by ion-exchange procedures. It is also possible that this property may induce changes in the electronic balance of the metal−support system, which in turn could have an impact on chemisorption and bond rupture of adsorbed reactant molecules, and consequently alter the selectivity. Other studies have highlighted the enhancement in catalyst dispersion arising from the support interaction when platinum and platinum−ruthenium particles were dispersed on graphitized carbon fibers.[12] Ross and co-workers[13] reported that carbon fibers could also be used as catalyst supports for transition metal oxides in hydrocarbon oxidation reactions.

In recent years, a new type of fibrous material has been developed by the use of catalytic carbon vapor deposition (CVD) techniques. This material, commonly known as carbon nanofi-

S1089-5647(97)03462-7 CCC: $15.00
Published on Web 02/27/1998

bers, consists of highly ordered graphite platelets oriented parallel, perpendicular, or at an angle with respect to the axis of the fibers where a large number of edges are exposed. A major advantage is that this type of carbon is relatively inexpensive to produce.[14] Carbon nanofibers generated from the decomposition of carbon-containing gases on metal surfaces have been the subject of much recent research in catalysis and materials science.[15−19] Under certain controlled conditions the growth of these structures can be catalytically engineered such that the product has the unique dual properties of high surface area, normally associated with amorphous active carbon supports, and a high degree of crystalline perfection more characteristic of graphite.[20] Furthermore, the orientation of the graphitic platelet component can be controlled by judicious choice of the catalyst, nature of the reactant gas, and the temperature at which the growth process is performed. It is this unusual combination of properties that makes carbon nanofibers an ideal candidate as a novel catalyst support medium. Previous work from this laboratory has shown that dramatic increases in catalytic activity for simple hydrogenation reactions were observed when copper−iron was dispersed on highly graphitic carbon nanofibers as compared to corresponding alumina and active carbon supported samples.[16] Other workers have also reported an increase in selectivity to cinnamyl alcohol in the hydrogenation of cinnamaldehyde when using ruthenium supported on carbon nanotubes as compared to more conventional support materials.[21] Geus and co-workers have reported that palladium supported on catalytically grown carbon fibers had comparable activity to that of an activated carbon supported palladium catalyst when studying liquid-phase nitrobenzene hydrogenation.[18] In the present study we have extended the earlier work conducted on the ethylene/hydrogen reaction[16] and have chosen the hydrogenation of 1-butene and 1,3-butadiene, respectively, as more demanding probe reactions in an attempt to monitor any possible changes in catalytic behavior induced by supporting nickel on a selection of traditional and carbon nanofiber support materials.

Early studies by Weisz and co-workers[22,23] highlighted the use of molecular sieve-supported catalysts for performing shape-selective chemical reactions. Using a 5A zeolite containing platinum, they demonstrated that it was possible to selectively hydrogenate 1-butene from a reactant mixture containing isobutene, since the larger sized latter molecules could not enter into caged structure of the support. This concept was later extended by Schmitt and Walker,[24] who investigated the use of platinum dispersed on carbon molecular sieve supports as a shape-selective hydrogenation catalyst system. They found that it was possible to selectively hydrogenate 1-butene and cyclopentene from mixtures of these respective olefins with 3-methyl-1-butene.

The hydrogenation of 1,3-butadiene has long been and continues to be employed in catalysis as a sensitive chemical probe of the surface of supported metallic catalysts.[25−31] Although there is a great deal of controversy concerning the working state of the catalyst and, in particular, the role that carbonaceous overlayers might play in the reaction,[32−35] the advantages of using this reaction are well documented. For a series of catalysts butadiene hydrogenation offers an ideal means of comparing simultaneously catalytic activity and selectivity. The catalytic semihydrogenation of dienes in alkene streams is also a vital industrial process. Palladium is usually the catalyst of choice for these selective hydrogenation reactions, but nickel has also been shown to form *n*-butenes selectively from 1,3-butadiene.[36,37] Wells and co-workers have noted two types of behavior for nickel catalysts: type A and type B nickel catalysts gave differing selectivities for the *n*-butenes, and this was later attributed to contamination of the nickel by adatoms such as sulfur or halogens.[37] The work presented here will demonstrate how large differences in the behavior of nickel for the hydrogenation of 1-butene and 1,3-butadiene can be induced by the nature of the catalyst support.

Experimental Section

Materials. Supported nickel catalysts were prepared by incipient wetness of fumed γ-alumina and active carbon, using a solution of nickel nitrate dissolved in deionized water to give a 5 wt % metal loading. Because of the hydrophobicity of the graphite nanofibers isobutyl alcohol was used as the solvent, but the metal loading was the same as that on the other supports. The impregnate was dried overnight in air at 110 °C, calcined in air at 400 °C for 4.0 h, and finally reduced in 10% hydrogen/helium for 20 h at 350 °C. After the reduction step, the samples were cooled to room temperature under flowing helium and then passivated in a 2% air/helium mixture for 1.0 h to prevent bulk oxidation of the nickel. The supported nickel catalysts were then removed from the reactor and stored in sealed vessels.

The graphite nanofibers used in this work were supplied by Catalytic Materials Ltd. and had a N_2 BET surface area of 184.0 m^2/g. Prior to use as a catalyst support media, the metallic impurities associated with the nanofibers were removed by dissolution in 1.0 M hydrochloric acid over a period of 3.0 days. The efficiency of this procedure was checked by performing X-ray diffraction analysis on the demineralized nanofibers, which showed the complete absence of any metallic components. Activated carbon was obtained from Norit and γ-alumina from Degussa and had N_2 BET surface areas of 516.6 and 91.2 m^2/g, respectively. The gases used in this study, 1-butene (99.99%), 1,3-butadiene (99.99%), hydrogen (99.999%), and helium (99.99%), were purchased from MG Industries, Inc. and were used without further purification. Reagent grade nickel nitrate [$(Ni(NO_3)_2 \cdot 6H_2O$] was obtained from Aldrich Chemicals.

Apparatus and Procedures. 1-Butene and 1,3-butadiene hydrogenation reactions were carried out in a vertical flow reactor system that was connected to an on-line Varian 3400 gas chromatography unit equipped with 30 m megabore columns (GS-Q). The reactor system consisted of a vertical Pyrex tube reactor (25 mm i.d. and 40 cm long) fitted with a frit at the midpoint and onto which 100 mg of the catalyst was placed. In this arrangement the hydrocarbon/hydrogen (1:2) reactant mixture was introduced at the top of the reactor and after passage through the catalyst bed exited at the bottom. Gas flow rates to the reactor were regulated by mass flow controllers (MKS). In all cases during a typical experiment, the catalyst samples were initially reduced in a 10% hydrogen/helium at 400 °C for 1.5 h, and then the temperature was lowered to the desired level of 80 °C for the subsequent hydrogenation reactions. A predetermined composition of reactant gas containing hydrocarbon, hydrogen, and helium, with the former two components being maintained at a 1:2 ratio, was introduced into the system at a flow rate of 100 cm^3/min and the reaction allowed to proceed for a period of 90 min, with gas product samples for analysis being taken at 5, 30, 60, and 90 min. The relative activity of each catalyst sample was determined from the percent total conversion of either 1-butene or 1,3-butadiene to gaseous products. Following the completion of a given reaction, the reactant gas was replaced by helium and the sample allowed to cool to room temperature. Before removal from the reactor, the sample was passivated according to the previously described procedure and then stored for later characterization studies.

An attempt was made to determine metal particle sizes by standard chemisorption procedures; however, this approach was fraught with problems and only gave meaningful data for the nickel particles dispersed on active carbon and γ-alumina. This result was not entirely unexpected since previous work from this laboratory has shown that a number of gases tend to be chemisorbed on graphite nanofibers,[38] and this behavior obscures the contribution that would be exhibited by any metal particles present on the material. In contrast, transmission electron microscopy examination of the samples proved to be a much more reliable method and provided not only information on the relative particle size distributions but also an insight into the variations in morphological characteristics displayed by the particles on the various support media.

Transmission electron microscopy examinations were performed in a JEOL 2000 EXII instrument (lattice resolution = 0.14 nm) that was equipped with a closed-circuit high-resolution television system. Suitable transmission specimens were prepared by ultrasonic dispersion of the catalyst samples in isobutyl alcohol and application of a drop of the suspension to a carbon support film. Images of these specimens were displayed on a TV monitor, and the high-magnification appearance of catalyst particles was recorded on videotape for subsequent direct transfer to a Mitsubishi printer unit. The size distribution of particles on the three different supports was determined from measurements of over 400 particles from a number of diverse regions of each specimen. In addition, morphological details of the particles and the manner by which the nature of the support influenced such features were obtained from careful inspection of many high-resolution electron micrographs. It should be appreciated that the majority of images obtained from conventional transmission electron microscopy are 2-dimensional in nature and as such does not allow one to determine the topographical characteristics of supported particles, i.e., overall shape and thickness. There are, however, exceptional situations where it is possible to observe the profile of particles located on edges of the support, and under these circumstances determination of the topographical features can be accomplished.

Results

1. Flow Reactor Studies. To ascertain the behavior of the pristine graphite nanofibers with respect to any possible intrinsic catalytic activity for the hydrogenation of either 1-butene or 1,3-butadiene, experiments were carried out with hydrocarbon/hydrogen mixtures over these structures for 90 min periods at 80 °C. There was no evidence to suggest that under these conditions the graphite nanofibers themselves were capable of promoting hydrocarbon conversion reactions.

1.1. Nickel Catalyzed Hydrogenation of 1-Butene. The results presented in Figures 1−3 show the total conversion of 1-butene at 80 °C and product distributions, expressed as mole fractions, as a function of reaction time for the three respective supported nickel catalysts. A somewhat more accurate assessment of the relative activities of these catalyst systems can obtained from a comparison of the respective turnover frequencies (TOF) that are presented in Table 1. These values have been estimated using the average metal particle sizes as determined from the TEM measurements. Also included in Table 1 are product selectivities, where S_2 = 2-butenes/2-butenes + butane and S_t = *trans*-2-butene/*cis*-2-butene, and all these values were determined after 60 min reaction time. It is evident that when nickel was supported on graphite nanofibers, the catalytic activity for hydrogenation of the olefin at 80 °C was appreciably higher than that found when the metal was supported on either active carbon or γ-alumina.

TABLE 1: Hydrogenation of 1-Butene over Supported Nickel Catalysts at 80 °C[a]

catalyst	TOF (s^{-1})	S_2[b]	S_t[c]
5 wt % Ni/graphite nanofibers	0.337	0.24	1.2
5 wt % Ni/active carbon	0.110	0.45	1.5
5 wt % Ni/γ-Al_2O_3	1.28×10^{-3}	0.11	1.4

[a] Reaction conditions: H_2/1-butene = 2.0; reaction time = 60 min; total pressure = 1 atm. [b] S_2 = 2-butene/(2-butene + butane). [c] S_t = *trans*-2-butene/*cis*-2-butene.

TABLE 2: Hydrogenation of 1,3-Butadiene over Supported Nickel Catalysts at 80 °C[a]

catalyst	TOF (s^{-1})	S_p[b]	S_1[c]	S_t[d]
5 wt % Ni/GNF	0.482	0.50	0.45	1.5
5 wt % Ni/active carbon	0.123	0.28	0.30	2.2
5 wt % Ni/γ-Al_2O_3	4.46×10^{-3}	0.05	0.40	2.0

[a] Reaction conditions: H_2/1,3-butadiene =2.0; reaction time = 60 min; total pressure = 1 atm. [b] S_p = butenes/(butenes + butane). [c] S_1 = 1-butene/(total butenes). [d] S_t = *trans*-2-butene/*cis*-2-butene.

1.2. Nickel-Catalyzed Hydrogenation of 1,3-Butadiene. In a further series of experiments the reactant gas was changed from 1-butene to 1,3-butadiene. The total conversion of 1,3-butadiene together with the mole fractions of hydrogenated gaseous products is plotted as a function of time for the three catalysts at 80 °C in Figures 4−6. In Table 2 values of the respective turnover frequencies are presented and were determined in a manner similar to those given in Table 1. In addition, various product selectivities are reported, where S_p = butenes/(butenes + butane), S_1 = 1-butene/(total butenes), and S_t = *trans*-2-butene/*cis*-2-butene. It can be seen that once again that graphite nanofiber supported nickel particles exhibited the highest activity for the diolefin hydrogenation reaction.

2. Catalyst Characterization Studies. Previous investigations from this laboratory have focused attention on the structural characteristics of graphite nanofibers derived from various catalyst/hydrocarbon reactant combinations, and it is germane to the current investigation to take into consideration the differences in the two types used as the support media. Graphite nanofibers produced from certain iron-catalyzed hydrocarbon decomposition reactions have been found to exhibit a highly crystalline structural form consisting of graphite platelets that are stacked in a perpendicular arrangement with respect to the axis of the fibers in an analogous manner to that of a pack of playing cards.[20] Furthermore, the oxidation characteristics of this material were almost identical to that of high-purity single-crystal graphite. Under these circumstances deposited nickel particles would be exclusively located at graphite edge sites. In contrast, the nanofibers generated from the cobalt-based catalysts took the form of multidirectional growths from a single catalyst particle, and their graphitic content was only about 25%.[19] In this case, one might expect to find that the probability for nickel particles to collect at preferred sites on the support surface was significantly lower than in the previous system.

2.1. Transmission Electron Microscopy Studies. Examination of the supported nickel catalysts in the transmission electron microscope revealed the existence of some dramatic differences in both the sizes and morphological characteristics of the metal particles in the three systems. The typical appearance of the nickel crystallites formed on the graphite nanofibers is shown in the electron micrograph (Figure 7). From a survey of many areas of the specimen it was evident that metal was evenly distributed over the nanofiber surface, and in general the particles adopted a well-defined hexagonal shape. In many

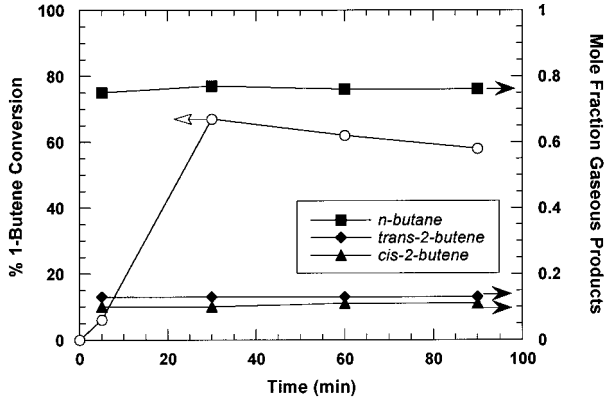

Figure 1. Percentage conversion of 1-butene and mole fraction of gaseous products as a function of reaction time in the presence of hydrogen over nickel dispersed on graphite nanofibers at 80 °C.

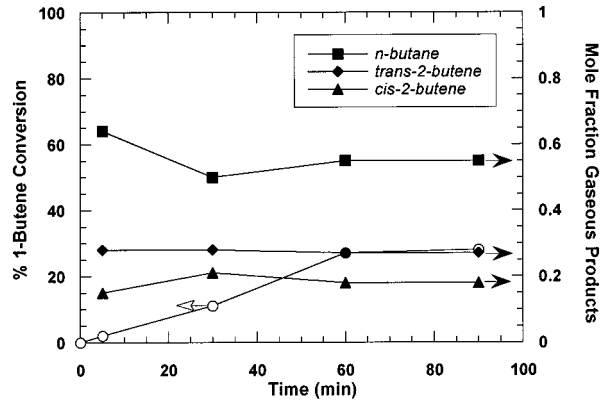

Figure 2. Percentage conversion of 1-butene and mole fraction of gaseous products as a function of reaction time in the presence of hydrogen over nickel dispersed on activated carbon at 80 °C.

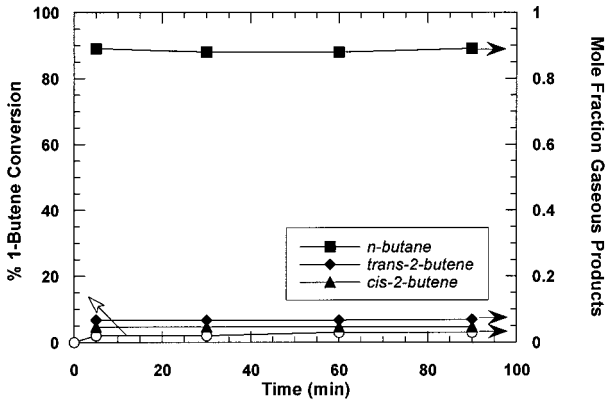

Figure 3. Percentage conversion of 1-butene and mole fraction of gaseous products as a function of reaction time in the presence of hydrogen over nickel dispersed on γ-alumina at 80 °C.

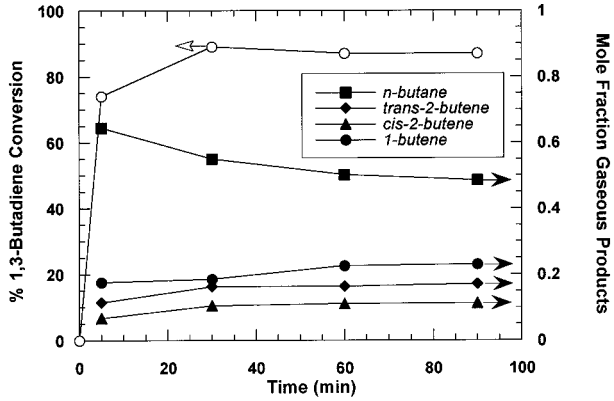

Figure 4. Percentage conversion of 1,3-butadiene and mole fraction of gaseous products as a function of reaction time in the presence of hydrogen over nickel dispersed on graphite nanofibers at 80 °C.

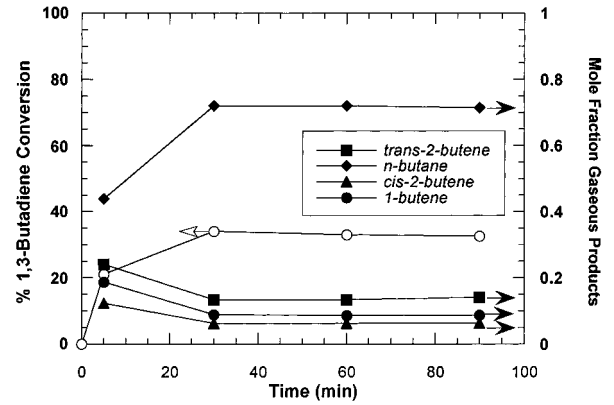

Figure 5. Percentage conversion of 1,3-butadiene and mole fraction of gaseous products as a function of reaction time in the presence of hydrogen over nickel dispersed on activated carbon at 80 °C.

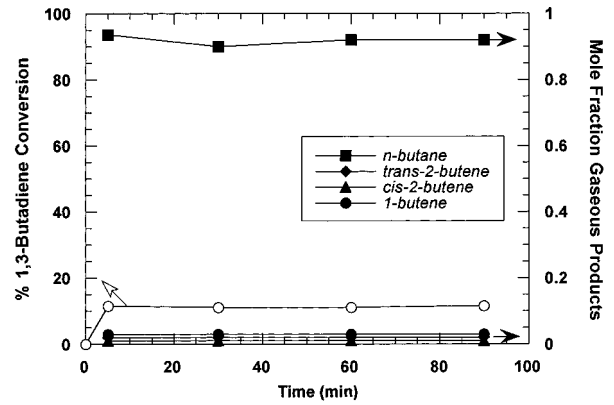

Figure 6. Percentage conversion of 1,3-butadiene and mole fraction of gaseous products as a function of reaction time in the presence of hydrogen over nickel dispersed on γ-alumina at 80 °C.

cases it was possible to discern features of the underlying support through the particles, indicating that they were relatively thin.

Inspection of many regions of active carbon supported nickel specimens showed that the metal was fairly evenly dispersed over the entire surface, and in this case the particles were significantly smaller on average than those deposited on the nanofiber support media. High-magnification studies revealed that the metal particles were highly faceted and tended to be very thin, flat structures. On scanning across the specimen, several different particle morphologies could be distinguished, including rectangular, pentagonal, and hexagonal shapes. There was no evidence to suggest that the particles adopted any preferred geometric form.

Finally, the appearance of nickel on γ-alumina (Figure 8) confirmed that when the metal was introduced onto a more traditional oxide catalyst support medium, then the most efficient dispersion was attained. It was apparent that not only was the distribution of metal crystallites extremely uniform over the whole surface but also the variation in particle size was extremely narrow. Perhaps the most dramatic feature was the fact that in the oxide supported nickel system the average particle size was about 5 times smaller than that for the same metal loading on the highly graphitic carbon nanofibers. It was also significant that even at very high magnification (6×10^6)

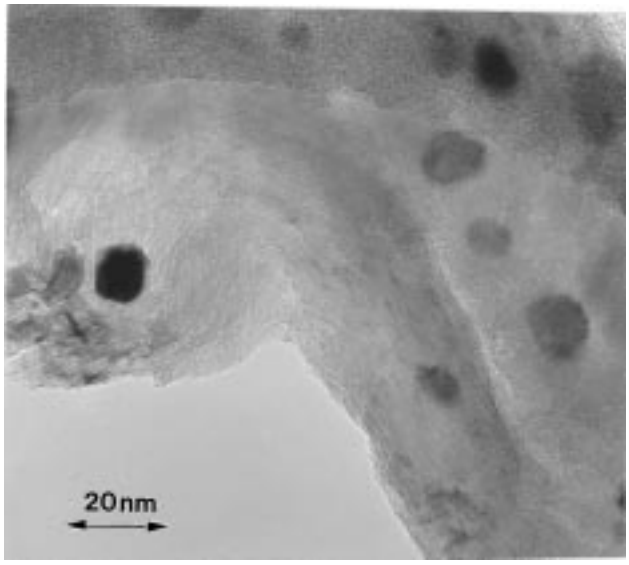

Figure 7. Transmission electron micrograph showing the appearance of metal crystallites generated on the graphite nanofibers.

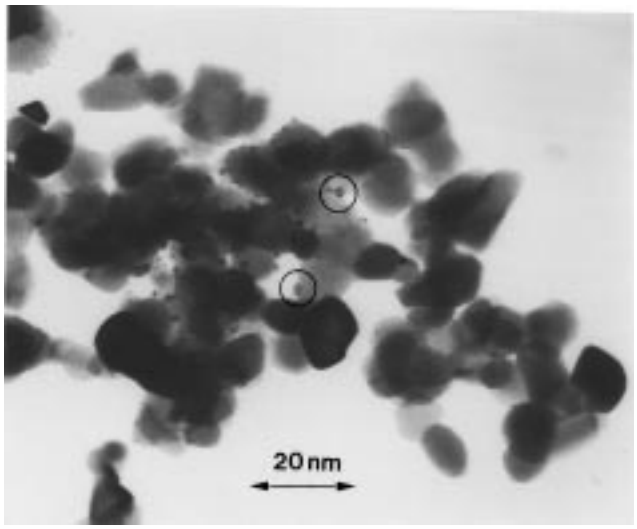

Figure 8. Transmission electron micrograph showing the appearance of metal crystallites produced on the γ-alumina support.

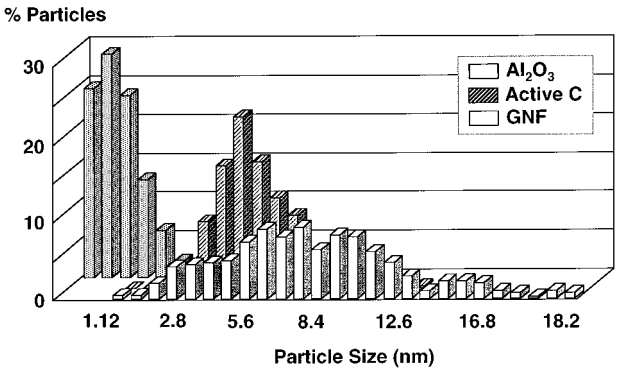

Figure 9. Particle size distribution of nickel crystallites dispersed on the three support media.

it was not possible to ascertain the detailed morphological characteristics of the metal particles in this system.

A clearer appreciation of the wide differences in the particle size distributions of nickel on these four support materials can be obtained from inspection of the data presented in Figure 9. It is apparent from examination of the data shown in this figure that the distribution profiles of nickel dispersed on the graphite nanofibers are in the range 2−22 nm. The nickel particle growth characteristics on active carbon and γ-alumina show behavioral patterns that are expected with these two support media, i.e., a very narrow size distribution being attained on the oxide and a somewhat broader profile existing on the carbonaceous material. It is significant to find that the latter particle size distribution is considerably more compact than that measured on the graphite nanofiber support. From these distributions it has been possible to derive the average metal particle sizes on the three supports, and the respective values are as follows: graphitic nanofibers, 8.1 nm; active carbon, 5.5 nm; and γ-alumina, 1.4 nm. It should be appreciated that since it was not possible to measure the sizes of particles below a lower limit of 0.35 nm, the analysis of these data will tend to give an overestimate of the values for the average particles sizes.

Discussion

A number of very intriguing findings, with regard to the potential advantages of employing graphite nanofibers as a support medium for metal particles for use as hydrogenation catalysts, have emerged from this investigation. It is evident that not only the activity but also the selectivity of nickel crystallites can be dramatically altered when the metal is dispersed on graphite nanofibers compared to the performance obtained with more traditional support materials, such as active carbon and γ-alumina. Consideration of the particle size distributions in conjunction with the catalyst reactivity data clearly demonstrates that hydrogenation of either 1-butene or 1,3-butadiene is not directly related to metal dispersion. If this parameter was the key factor in determining catalyst activity, then one would expect that the nickel/γ-alumina system should exhibit the highest reactivity and that when the metal was supported on graphite nanofibers a somewhat inferior performance would be realized. The fact that the experimental data are not consistent with this argument suggests that other factors are operative in these reactions. In the ensuing discussion we shall endeavor to link these differences in the behavioral patterns of the catalyst systems with the observed modifications in metal particle morphological characteristics induced by the chemical and structural properties of the support materials.

Transmission electron microscopy examinations show that nickel particles deposited on the graphitic nanofibers adopt morphologies that are generally associated with the existence of a strong metal−support interaction. The crystallites tend to be relatively thin and flat hexagonal-shaped structures—features that are consistent with the characteristics predicted from the spreading action of metal species on the support. Under these circumstances it is expected that only certain metal faces will be exposed and available for interaction with gaseous reactant molecules. While the results of the electron microscopic examinations of the carbon nanofiber supported nickel catalysts do not allow us to reach any definitive conclusions with regard to the possibility of preferred growth locations for the metal particles, previous studies of the nickel/graphite−hydrogen system may provide some relevant information on this matter.[39−42] Using controlled atmosphere electron microscopy techniques, it was possible to continuously follow the creation of channels across the graphite basal plane by nickel particles when the specimens were heated in the presence of hydrogen. Detailed analysis of the recorded sequences showed that the channels possessed many straight sections interrupted by changes in direction of 60° or 120° and were oriented parallel to the (1120) crystallographic directions. A further observation of great significance was that a thin film of nickel strongly adhered to

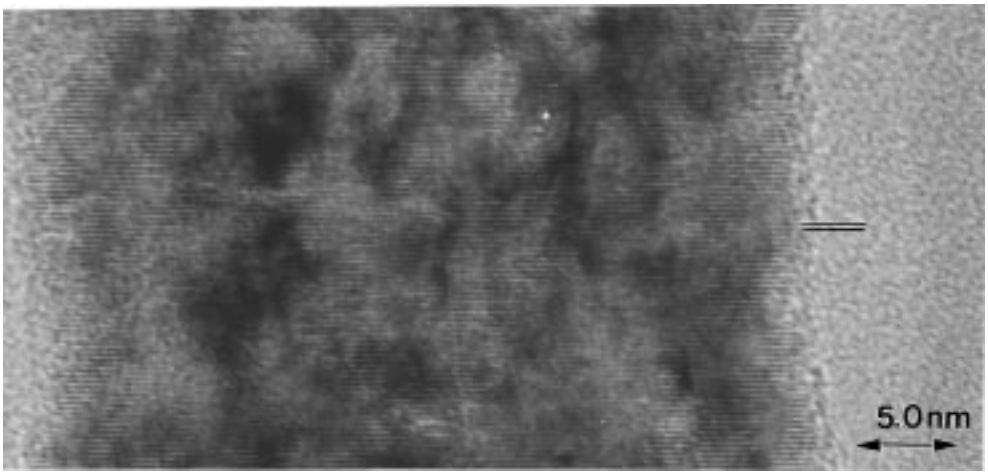

Figure 10. High-resolution transmission electron micrograph showing the arrangement of the graphite platelets stacked in a direction perpendicular to the fiber axis and separated by a distance of 0.34 nm.

the walls of the channel was being left behind, a clear indication that in a hydrogen environment nickel will preferentially wet and spread along the "armchair" face.[42] It can be concluded that since nickel establishes a very strong interaction with the carbon atoms located at the "armchair" face, its interaction with those at the "zigzag" face are somewhat weaker,[43] and therefore, one could speculate that the metal particles will adopt a different morphology at each of the crystal faces. These features will be the subject of a further study in which the metal is dispersed on various types of nanofibers where the graphite planes are orientated in different directions with respect to the fiber axis.

Inspection of the data presented in Figures 1−6 and Tables 1 and 2 clearly demonstrates that when nickel is supported on graphite nanofibers a greater catalytic activity is achieved for the hydrogenation of both 1-butene and 1,3-butadiene than that observed for the same metal loading on either active carbon or γ-alumina. It is apparent from the selectivity patterns that the highest yields of *trans*- and *cis*-2-butenes are obtained with a nickel/active carbon catalyst, indicating that isomerization is more prevalent when the metal is supported on this medium rather than on the graphite nanofibers or γ-alumina. While butane was observed to be the major product for the 1,3-butadiene hydrogenation for all the supported nickel systems, there was a higher selectivity toward the formation of the partially hydrogenated butenes when metal was dispersed on the nanofibers. It is significant that for all the catalyst systems the *trans*-2-butene/*cis*-2-butene ratios obtained from hydrogenation of the diolefin are in the range 1.5−2.2, and these values are consistent with those reported in the literature for supported nickel catalysts.[36,37,44] An exhaustive search of the literature has failed to reveal the existence of any data pertaining to the relationship between nickel particle size effects and the hydrogenation of olefins; however, it is reasonable to assume that the reactions are quite facile.

It would be appropriate to initially consider some of the fundamental structural features that make graphite nanofibers a unique catalyst support material. Graphite consists of stacked layers of carbon atoms, arranged in a symmetrical hexagonal distribution, separated from each other by a distance of 0.335 nm. Three main faces can be identified: the basal plane (002) possessing an associated cloud of delocalized π-electrons and two prismatic faces where the carbon atoms are arranged in either "zigzag" $\{10\bar{1}0\}$ or "armchair" $\{11\bar{2}0\}$ orientations. The nanofibers can be synthesized as to produce a structural conformation consisting of a perfect array of graphite platelets where the exposed regions consist almost entirely of edges, as

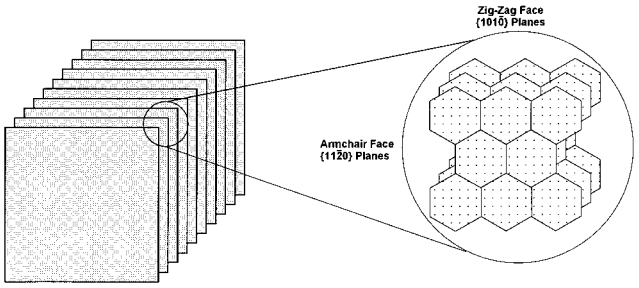

Figure 11. Schematic representation of the stacking order of graphite platelets in the nanofibers and a detailed view of the difference in carbon atom arrangement in the prismatic faces.

shown in the high-resolution transmission electron micrograph (Figure 10). The graphite nanofibers used in the present investigation have therefore the two sets of prismatic faces exposed, and it is these specific regions that will be available for interaction with the deposited metal atoms. The conformation of this novel material is to be contrasted with that encountered in traditional graphitic materials, where the major fraction of the exposed structure consists of basal plane regions with a smaller fraction of available reactive edge sites.

A more detailed understanding of the structural arrangement and crystallographic features of the graphite platelets can be obtained from examination of the schematic representation (Figure 11), where the 3-D graphite platelet view has been enlarged so to permit a more detailed appreciation of the crystallographic arrangement. The distribution of carbon atoms in the $(10\bar{1}0)$ and $(11\bar{2}0)$ faces as well as the distance between atoms and layers and the relative size of a nickel atom are shown in Figure 12. A close scrutiny of these two models reveals that there is a significant difference in the topographical characteristics of the respective faces, with surface a presenting a more open structure than surface b, which will induce a different distribution of nickel atoms on the crystal surface. It is therefore not unreasonable to expect that the metal particles that are subsequently deposited on these surfaces will exhibit dissimilar morphologies and concomitant variations in catalytic behavior. Indeed, in cases where a strong interaction exists between the metal atoms and the graphitic support, it would be possible for the crystallites to form an epitaxial relationship with the surface carbon atoms and adopt the crystallographic character of the particular face, where metal atoms would be arranged so to create a structure that is relatively open and, as such, favor an increase in the sticking coefficient of reactant molecules. It is

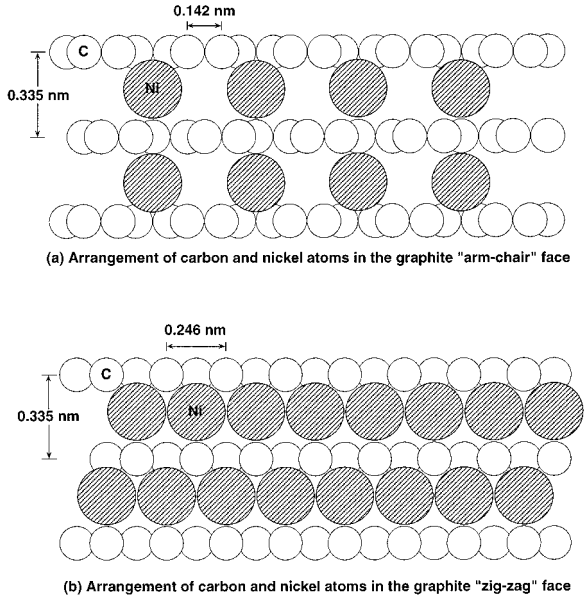

Figure 12. Schematic representation showing the possible accommodation of nickel atoms on the two prismatic faces of graphite.

not unreasonable to assume that graphite platelets could provide a template for the generation of metal particle structures possessing a more accessible surface with a smaller coordination number that in turn produces a narrower d-band and accordingly a more stable adsorbate. Since the crystalline perfection of the graphite nanofibers is quite extensive, this type of strong metal−support interaction is expected to exist over a wide range of nickel crystallite sizes.

In addition to the geometric constraints imposed on the particles by the support, a further important issue to be considered with respect to graphite is the presence of delocalized π-electrons that are responsible for bestowing the electrical conductive properties on the material. This aspect raises the possibility that electron transfer can take place between the metal and the graphitic nanofiber support, and this action can impart unusual properties to the catalyst particles. The concept of electron transfer from the support to metal crystallites was invoked by Richard and co-workers[8,45] to account for the observed enhancement in activity when platinum was supported on graphite for the cinnamaldehyde hydrogenation. It was claimed that the electronic effect was responsible for inducing an expansion of the platinum lattice and a decrease in the ratio of adsorption coefficients of toluene and benzene on the modified metal surface. It is well-known that when two solid surfaces are brought into contact, flow of electrons from the material possessing the higher work function to the one with the lower value will occur. This principle is widely used in a variety of electrical devices. In the present system nickel particles deposited on graphitic nanofibers will be electronically perturbed by the interaction with the support.

Electronic effects on catalysis have received considerable attention in recent years,[46,47] and indeed, the significance of electrostatic effects and charge transfer between preadsorbed electronegative and electropositive adatoms on the adsorption properties of simple molecules have been shown in a number of theoretical papers.[48,49] It is recognized that such perturbations will affect the manner by which the adsorbate will be chemisorbed and whether it would subsequently undergo dissociation. In the present investigation it can be argued that if graphite donates electrons to the metal, the occupancy of antibonding states in the gaseous reactant such as hydrogen can be increased ($s \rightarrow s^*$), and this will lead to the dissociation of the molecules into chemisorbed atoms. Conversely, if electrons are withdrawn from the metal to the graphite, activation of the surface for the interaction with the π-bonds in the hydrocarbon can be affected. The electronic effect has been invoked to explain the high reactivity of sulfur-contaminated catalysts in the conversion of 1,3-butadiene to *trans*-2-butene observed by George and co-workers.[37] Other workers[50] studied the effects of various adatoms including boron, phosphorus, aluminum, and sulfur on the hydrogenation activity of nickel and concluded that the catalytic properties of the metal drastically changed as a function of the electronic density of nickel.

One must also be aware that the possibility exists for reactant gas molecules and particularly those containing C=C bonds to interact with the graphite edge regions. This factor could exert an impact on the events occurring at the metal/graphite nanofiber interface. As a consequence, some of the observed differences in reactivity between graphite nanofibers and active carbon supported metal particles might be attributable to the participation of the supporting medium in the hydrocarbon conversion reaction. It should be stressed, however, that hydrocarbon adsorption experiments performed in the absence of the nickel component failed to show any differences in the behavior of the three support materials.

Acknowledgment. Support for this project was provided by NSF Grant CTS-9222572, and financial assistance for N.M.R. was provided by the New Energy and Industrial Development Organization (NEDO) of Japan.

References and Notes

(1) Adadurov, I. J. *J. Phys. Chem. USSR* **1935**, *6*, 206.
(2) Schwab, G. M. *Adv. Catal.* **1978**, *27*, 1.
(3) Baker, R. T. K.; Tauster, S. J.; Dumesic, J. A. *Strong Metal Support Interactions;* ACS Symposium Series 298; American Chemical Society: Washington, DC, 1986.
(4) Bond, G. C.; Burch, R. *Catalysis*; The Royal Society of Chemistry: London, 1983; Vol. 6, p 27.
(5) Stevenson, S. A.; Dumesic, J. A.; Baker, R. T. K.; Ruckenstein, E. *Metal-Support Interactions in Catalysis, Sintering and Redispersion;* Van Nostrand Reinhold Co.: New York, 1987.
(6) Haller, G. L.; Resasco, D. E. *Adv. Catal.* **1991**, *132* , 269.
(7) Brownlie, I. C.; Fryer, J. R.; Webb, G. *J. Catal.* **1969**, *14* , 263.
(8) Richard, D.; Fouilloux, P.; Gallezot, P. *Proc. 9th Int. Congr. Catal.* **1988**, 1074.
(9) Gallezot, P.; Richard, D.; Bergeret, G. In *Novel Materials in Heterogeneous Catalysis;* Baker, R. T. K., Murrell, L. L., Eds.; ACS Symposium Series 437; American Chemical Society: Washington, DC, 1990; p 150.
(10) Kuroda, A.; Aizawa, H.; Masubichi, Y.; Ishihara, G.; Matsuhisa, S.; Taira, S. Jap. Patent 50/15754, 1973.
(11) Theodoridou, E.; Jannakoudakis, A. D.; Besenhari, J. J.; Sauter, R. F. *Synth. Met*. **1986**, *14*, 125.
(12) Mahmood, T.; Williams, J. O.; Miles, R.; McNicol, B. D. *J. Catal.* **1981**, *72*, 218.
(13) Ross, R. A.; Fairbridge, C.; MacCallum, J. R. *Carbon* **1985**, *23*, 209.
(14) Rodriguez, N. M. *J. Mater. Res*. **1993**, *8*, 3233.
(15) Fenelonov, V. B.; Avdeeva, L. B.; Zheivot, V. I.; Okkel, L. G.; Goncharova, O. V.; Pimneva, L. G. *Kinet. Catal*. **1993**, *34* , 483.
(16) Kim, M. S.; Rodriguez, N. M.; Baker, R. T. K. *J. Phys. Chem.* **1994**, *98*, 13108.
(17) Shaikhutdinov, S. K. *Kinet. Catal*. **1995**, *36*, 549.
(18) Hoogenraad, M. S.; van Leeuwarden, R. A. G. M. M.; van Breda Vriesman, G. J. B.; Broersma, A.; van Dillen, A. J.; Geus, J. W. *Stud. Surf. Sci. Catal.* **1995**, 263.
(19) Chambers, A.; Rodriguez, N. M.; Baker, R. T. K. *J. Mater. Res.* **1996**, *11*, 430.
(20) Rodriguez, N. M.; Chambers, A.; Baker, R. T. K. *Langmuir* **1995**, *11*, 3862.
(21) Planeix, J. M.; Coustel, N.; Coq, B.; Brotons, V.; Khumbhar, P. S.; Dutartre, R.; Genests, P.; Bernier, P.; Ajayan, P. M. *J. Am. Chem. Soc.* **1994**, *116*, 7935.
(22) Weisz, P. B.; Frilette, V. J. *J. Phys. Chem.* **1960**, *64*, 382.

(23) Weisz, P. B.; Frilette, V. J.; Mattman, R. W.; Mower, E. G. *J. Catal*. **1962**, *1*, 307.
(24) Schmitt, J. L., Jr.; Walker, P. L., Jr. *Carbon* **1972**, *10*, 87.
(25) Meyer, E. F.; Burwell, R. L. *J. Am. Chem. Soc.* **1963**, *85*, 2881.
(26) Bond, G. C.; Webb, G.; Wells, P. B.; Winterbottom, J. M. *J. Chem. Soc. A* **1965**, 3218.
(27) Nishimura, E.; Inoue, Y.; Yasumori, I. *Bull. Chem. Soc. Jpn.* **1975**, *48*, 803.
(28) Furlong, B. K.; Hightower, J. W.; Chan, T. Y.-L.; Sarkany, A.; Guczi, L. *Appl. Catal.* **1994**, *117*, 41.
(29) Miegge, P.; Rousset, J. L.; Tarby, B.; Massardier, J.; Bertolini, J. C. *J. Catal.* **1994**, *149*, 404.
(30) Lee, K. H.; Wolf, E. E. *Catal. Lett.* **1994**, *26*, 297.
(31) Sarkany, A.; Zsoldos, Z.; Stefler, G.; Hightower, J. W.; Guczi, L. *J. Catal*. **1995**, *157*, 179.
(32) Al Ammar, A. S.; Webb, G. *J. Chem. Soc., Faraday Trans. 1* **1978**, *74*, 195.
(33) Al Ammar, A. S.; Webb, G. *J. Chem. Soc., Faraday Trans. 1* **1978**, *74*, 1900.
(34) Gardner, N. C.; Hansen, R. S. *J. Phys. Chem.* **1970**, *74*, 3298.
(35) Thomson, S. J.; Webb, G. *J. Chem. Soc., Chem. Commun.* **1976**, 526.
(36) Phillipson, J. J.; Wells, P. B.; Wilson, G. R. *J. Chem. A* **1969**, 1351.
(37) George, M.; Moyes, R. B.; Ramanarao, D.; Wells, P. B. *J. Catal.* **1978**, *52*, 486.
(38) Park, C.; Chambers, A.; Baker, R. T. K.; Rodriguez, N. M. *J. Phys. Chem. B*, in press.
(39) Tomita, A.; Tamai, Y. *J. Phys. Chem.* **1974**, *76*, 2254.
(40) Keep, C. W.; Terry, S.; Wells, M. *J. Catal.* **1980**, *66*, 451.
(41) Baker, R. T. K.; Sherwood, R. D. *J. Catal.* **1981**, *70*, 198.
(42) Baker, R. T. K.; Sherwood, R. D.; Derouane, E. G. *J. Catal.* **1982**, *75*, 382.
(43) Abrahamson, J. *Carbon* **1973**, *11*, 337.
(44) Sarkany, A.; Schay, Z.; Steffler, G.; Borko, L.; Hightower, J. W.; Guczi, L. *Appl. Catal. A* **1995**, *124*, L181.
(45) Gallezot, P.; Leclercq, C.; Mutin, I.; Nicot, C.; Richard, D. *J. Microsc. Spectrosc. Electron*. **1985**, *10*, 479.
(46) Norskov, J. K. *Prog. Surf. Sci*. **1991**, *38*, 103.
(47) Somorjai, G. A. *Introduction to Surface Chemistry and Catalysis;* John Wiley & Sons: New York, 1994.
(48) Schultz, P. A.; Patterson, C. H.; Messmer, R. P. *J. Vac. Sci. Technol.* **1987**, *A5*, 1061.
(49) Muller, J. E. In *Physics and Chemistry of Alkali Adsorption*; Bonzel, H. P., Bradshaw, A. M., Ertl, G., Eds.; Elsevier Science Publishers: Amsterdam, 1989.
(50) Okamoto, Y.; Fukino, K.; Imanaa, Teranishi, S. *J. Catal*. **1982**, *74*, 173.